Atomic structure of the CdS(11$\bar{2}$0) surface: A dynamical analysis of low-energy electron-diffraction intensities

A. Kahn
Department of Electrical Engineering, Princeton University, Princeton, New Jersey 08544

C. B. Duke and Y. R. Wang
Xerox Webster Research Center, 800 Phillips Road, Webster, New York 14580

(Received 9 October 1990)

A determination of the atomic geometry of the CdS(11$\bar{2}$0) surface by dynamical analysis of measured low-energy ($35 \leq E \leq 250$ eV) electron-diffraction (LEED) intensities is reported. The analysis is performed on the average of two data sets, each of which includes fifteen diffracted beams. Intensities are measured from two different CdS surfaces cleaved in ultrahigh vacuum and cooled below 50 K. The measurements are made using a fast LEED data-acquisition system. The scattered intensities are calculated using a relativistic, energy-dependent Hara-exchange electron–ion-core potential. The search for the best-fit structure is conducted with a combination of the x-ray R factor and integrated-intensity R factor. The best description of the experimental intensities by the calculated ones is obtained for a structure characterized by a bond-length-conserving relaxation of the surface Cd-S-Cd and S-Cd-S triplets by an angle $\omega = 30°$ followed by a 0.1 Å contraction of the first layer toward the bulk. This structure is in quantitative agreement with predictions based on total-energy-minimization calculations for this surface.

I. INTRODUCTION

The atomic geometry and electronic structure of the nonpolar (10$\bar{1}$0) and (11$\bar{2}$0) cleavage faces of II-VI wurtzite-structure compounds have recently become topics of renewed interest.[1–3] In addition to providing surface-structure determinations for individual members of this important class of semiconductors, these studies permit a comparison of the surface relaxation mechanisms with those operating on the (110) cleavage surfaces of zinc-blende-structure compound semiconductors. The atomic relaxation on (110) zinc-blende-structure surfaces is driven by a lowering of the surface electron energy.[4] The rehybridization of the surface bonds that accompanies a bond-length-conserving rotation of the top-layer atoms moves the filled anion- and empty cation-derived dangling-bond states into the valence and conduction band, respectively, resulting in a sizable decrease of the surface electronic energy. This behavior, which results from a combination of the possibility of bond-length-conserving relaxations of surface species and the elimination of dangling-bond surface states characteristic of the truncated-bulk geometry, also has been predicted by total-energy-minimization calculations for cleavage surfaces of wurtzite-structure compounds.[3] These calculations predicted a set of surface geometries for several materials that are compatible with those extracted from the low-energy electron-diffraction (LEED) and low-energy positron-diffraction (LEPD) studies of the (10$\bar{1}$0) and (11$\bar{2}$0) surfaces of CdSe.[2,5]

Atoms on (10$\bar{1}$0) and (11$\bar{2}$0) wurtzite-structure surfaces exhibit quite different connectivities. On the (10$\bar{1}$0) surface, each atom is bound to one surface and two second-layer atoms, and the local structure corresponds to anion-cation dimers parallel to the [0001] direction. On the (11$\bar{2}$0) surface, each atom is bound to two surface and one second-layer atom, and the local structure is that of zigzag chains that extend along the [0001] direction (Fig. 1). Nevertheless, the topology of these surfaces permits the construction of bond-length-conserving local atomic distortions, which are similar to each other as well as to those observed on (110) surfaces. In all cases, the total-energy calculations indicate that these local bond-length-conserving distortions of surface atoms in which the top-layer anion and cation are displaced away from and toward the bulk, respectively, generate the electronic energy that drives the surface relaxation. This relaxation is accompanied by a strengthening of the back bonding between the surface anions and the cations of the second layer driven by rehybridization of the surface bonding upon rotation of the surface species.

While the experimental LEED and LEPD results for CdSe are encouraging, they do not establish the generality of the phenomena noted above. In order to expand the scope of such experimental results, we present here a determination of the atomic geometry of CdS(11$\bar{2}$0) by full dynamical analysis of LEED intensities. The results reveal clearly that the surface is relaxed and that the structure is very close to that prediced by theory. It is described in terms of a rotation of surface bonds in which the anions and cations are displaced upward and downward, respectively, followed by a small rigid contraction of the relaxed top layer toward the bulk. Within the accuracy of the analysis, no second-layer distortion is detected.

We proceed with the description of the experiment and of the model calculations used to analyze the LEED intensities. The results of the analysis are given in the final section.

 ©1991 The American Physical Society

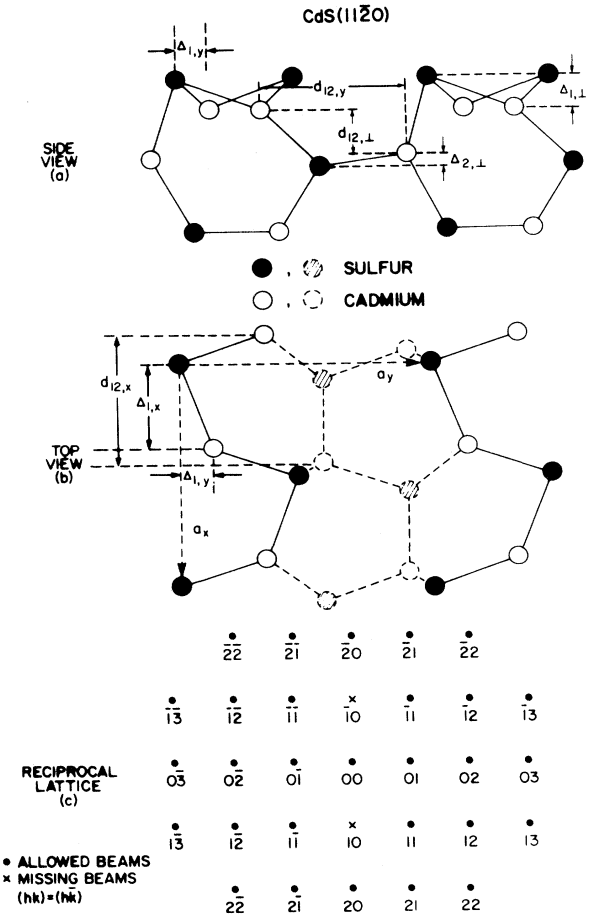

FIG. 1. Schematic representation of the wurtzite-structure lattice showing (a) the side view and (b) the top view of the geometry of the relaxed CdS(11$\bar{2}$0) surface. A schematic indication of the normal-incidence LEED pattern is given in (c). The independent structural variables are defined in (a) and the dimensions of the unit cell (Ref. 17) are given in (b).

II. EXPERIMENT

Low-resistivity CdS single crystals in the form of bars 5×5×16 mm with the long axis along the [11$\bar{2}$0] direction were purchased from Cleveland crystals. The bars were cleaved in ultrahigh vacuum (10^{-10} Torr) to expose fresh surfaces and cooled below 50 K to reduce thermal atomic vibrations and improve the signal-to-background ratio during LEED intensity measurements. No surface charging was observed. LEED measurements were performed with a four-grid LEED optics. The intensities were measured with a fast LEED computer-based data-acquisition system using a Dage-MTI camera. The intensity profiles of fifteen beams were collected in energy steps of 2 eV and for energies ranging from about 35 to 250 eV. The total elapsed time of beam exposure for data collection was about 10 min. Two sets of data were collected, one from each of two different cleaves. The average of these sets is used for the analysis. The diffraction pattern exhibited the $(hk)=(h\bar{k})$ symmetry and the absence of intensity in the $(h0)$ beams for odd h resulting from the glide-plane symmetry of the (11$\bar{2}$0) unit cell. The discussion of this symmetry is given in Appendix A. Each set of intensity data included those beams with indices $(\bar{1}1)=(1\bar{1})$, $(11)=(\bar{1}\bar{1})$, $(01)=(0\bar{1})$, $(\bar{2}0)$, (20), $(02)=(0\bar{2})$, $(21)=(2\bar{1})$, $(\bar{1}2)=(1\bar{2})$, $(12)=(\bar{1}\bar{2})$, $(\bar{2}\bar{2})=(22)$, $(22)=(2\bar{2})$, $(\bar{2}1)=(2\bar{1})$, $(\bar{3}1)=(3\bar{1})$, $(\bar{1}3)=(1\bar{3})$, and $(13)=(\bar{1}\bar{3})$. We found that the diffracted beams could be divided into strong beams [(11), ($\bar{1}$1), (01), ($\bar{2}$0), (20), and ($\bar{1}$2)], medium beams [(21), (12), ($\bar{2}$2), and ($\bar{3}$1)], and weak beams [(22), (02), ($\bar{2}$1), (13), and ($\bar{1}$3)]. A diagram of the surface unit-cell geometry and beam indices is given in Fig. 1.

III. MODEL CALCULATIONS

A multiple-scattering model of the electron-diffraction process, described previously,[6] was used to perform the dynamical calculations of the LEED intensities for the given surface atomic geometries. In this model, the scattering species are represented by energy-dependent phase shifts in terms of which the LEED intensities are computed. Each atomic layer parallel to the surface is divided into two Cd and two S sublattices. Each two-dimensional surface unit cell includes one atom from each of these four primitive sublattices (Fig. 1). The scattering amplitudes for each sublattice are evaluated analytically, whereas the scattering between sublattices is described by a set of coupled matrix equations expressed in the angular momentum representation.[7] These equations are solved exactly for a prescribed number of the top layers that is varied until convergence is achieved. For deeper layers, the scattering amplitudes for each layer are obtained by considering the multiple scattering between the four sublattices within the layer but neglecting the multiple scattering between layers. The LEED intensities are expressed as a superposition of the scattering amplitudes for the individual layers calculated as indicated above.[1,6,7]

The electron-ion-core interaction is described by a one-electron muffin-tin potential. The one-electron crystal potential is formed from a superposition of overlapping neutral (i.e., Cd and S) relativistic charge densities. These charge densities are obtained via self-consistent solutions to the Dirac equation for the individual atomic species. Given the charge densities, the phase shifts are evaluated by solving the nonrelativistic Schrödinger equation using the energy-dependent Hara model of the exchange potential with a muffin-tin approximation of the crystal potential.[8,9] The anion and cation muffin-tin radii correspond to the point at which the potentials of Cd and S nearest neighbors cross. Outside the muffin-tin spheres, the potential is taken to be the calculated value at the crossover point. Because the exchange potential depends on the energy of the incident electron, the muffin-tin radii also depend on incident energy. In the 35–250-eV energy range considered here, however, these radii are practically constant and equal to 1.33 and 1.26 Å for Cd and S, respectively. The calculated phase shifts associated with these parameters are shown in Fig. 2.

In the calculation, the electron-electron interaction is

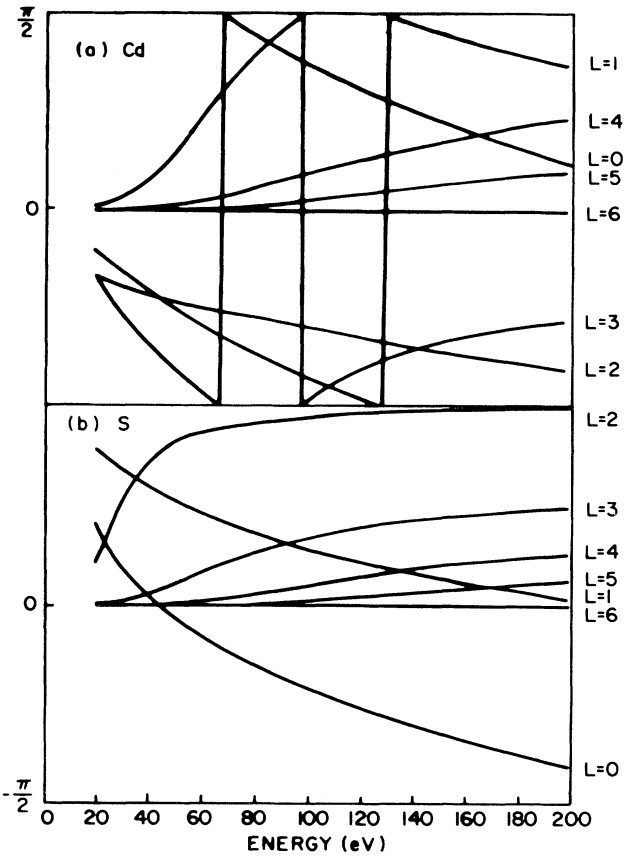

FIG. 2. Phase shifts for (a) Cd and (b) S in CdS resulting from using the Hara exchange (Ref. 8) in the self-consistent atomic potential calculated as described in the text.

taken into account via a complex optical potential $\Sigma(E) = -V_0 + iV_i$, where V_0 is a constant, real inner potential, and V_i is characterized by the inelastic mean free path λ_{ee}.[10] The fit between experimental and calculated intensity versus energy (I-V) profiles is quantified with the x-ray R factor [R_X given by Eqs. (3), (8), (13), (14), and (16) of Ref. 11] and the integrated-intensity R factor[12] (R_I). The latter gives a measure of how the calculation meets the relative strength of various beams. For each calculation, V_0 was selected to minimize R_X. V_0 was always found approximately equal to 10 eV.

An initial structure search, described in more detail below, was performed using an inelastic collision mean free path $\lambda_{ee} = 10$ Å, six phase shifts for each scatterer, and a slab of six layers (four subplanes in each layer) in which the diffraction from the top three was calculated exactly. Convergence tests for the CdS(11$\bar{2}$0) surface revealed that an accuracy of better than 1% in the R factors could be achieved with $\lambda_{ee} = 10$ Å, six phase shifts, a slab of seven layers, and four layers calculated exactly. Following the initial structure search, we subsequently verified that this more complete calculation led to the same structure as that obtained with the less expensive six-layer calculation, insuring that our results were converted. Finally, since the experiment was performed with the sample cooled below 50 K, we neglected the effect of thermal lattice vibrations in the calculations.

IV. STRUCTURE ANALYSIS

The analysis of the LEED intensity data to obtain the CdS(11$\bar{2}$0) surface geometry was analogous to those previously used to determine atomic geometries of III-V and II-VI cleavage surfaces. The diffracted beam intensities corresponding to the unrelaxed, or bulk-truncated, geometry were calculated first and compared with experiment. The parameters specifying this unrelaxed geometry are presented in Table I. The resulting values of R_X and R_I were found to be 0.27 and 0.29, respectively. Although these results indicate a reasonable description of the line shape of the experimental I-V profiles by the calculated ones ($R_X < 0.3$), they reveal a poor fit of the relative integrated intensities of various beams ($R_I > 0.15$). Examples of the comparison of the calculated and measured I-V profiles are given in Fig. 3. Consequently, a search of the structure parameter space was conducted in an attempt to improve the model description of the experimental intensities.

An important feature of the cleavage faces of the tetrahedrally coordinated compound semiconductors is their exhibition of bond-length-conserving relaxations, which alter the local bonding conformation of the surface anions and cations without the need to pay the energy price of bond-length modification.[1-5] Thus, the surface-structure searches were initiated by defining these relaxations in terms of dimensionless angular variables and initially searching the space defined by these variables before examining bond-length-distorting relaxations. For wurtzite structure (11$\bar{2}$0), there are two independent angular structural variables, the angles of rotation of the normals to the planes defined by Cd-S-Cd triplets (ω_A) and S-Cd-S triplets (ω_C), respectively, as discussed in Appendix B. To achieve a single variable initial analysis we select one of these, $\omega = \omega_C$, as the independent variable and use an empirical constitutive relation to relate ω_A to

TABLE I. Structural parameters specifying the atomic geometry of CdS(11$\bar{2}$0). All are defined in Fig. 1.

Structure	a_x (Å)	a_y (Å)	$\Delta_{1\perp}$ (Å)	D_{1x} (Å)	Δ_{1y} (Å)	$d_{12\perp}$ (Å)	d_{12x} (Å)	d_{12y} (Å)	$\Delta_{2\perp}$ (Å)	ω (deg)	V_0 (eV)	R_X	R_I
Unrelaxed	6.749	7.162	0	2.532	0	2.067	3.375	3.58	0	0	10	0.27	0.29
$\omega = 32°$	6.749	7.162	0.69	3.28	0.52	1.56	3.81	3.92	0	32°	10	0.25	0.095
"Best fit"	6.749	7.162	0.65	2.39	0.51	1.50	3.77	3.91	0	30°	10	0.21	0.083
Theory	6.749	7.162	0.69	2.33	0.51	1.47	3.71	4.04	0.11				

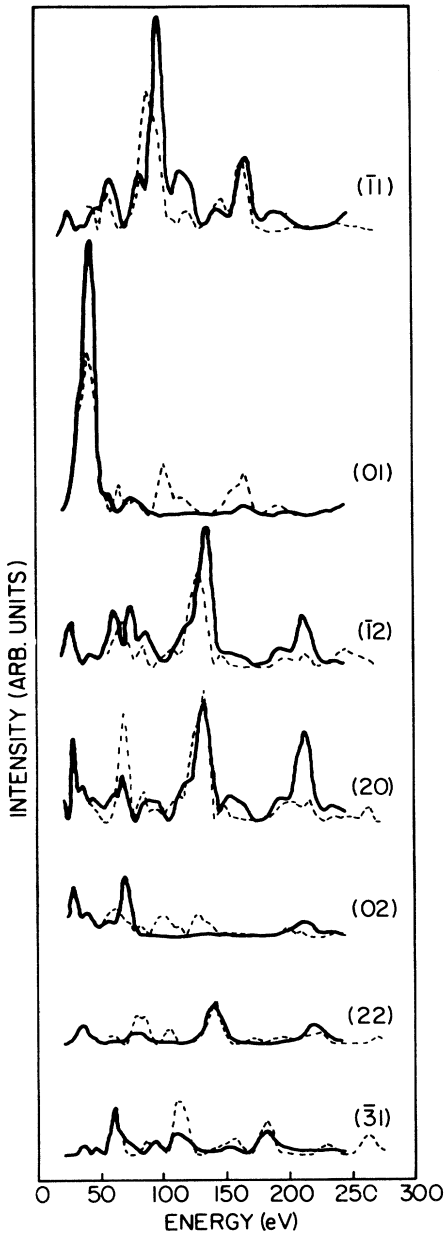

FIG. 3. Comparison between calculated (solid line) and measured (dashed line) intensities of normally incident electrons on CdS(11$\bar{2}$0) diffracted into various beams. The calculated intensities correspond to the unrelaxed surface, as specified in the top row of Table I.

ω based on total-energy calculations.[3] Hence, the specification of ω defines the structural parameters for bond-length-conserving relaxations. The relation between ω and $\Delta_{1\perp}$, the shear perpendicular to the surface between Cd and S in the top layer, $\Delta_{1\parallel}$, the relative displacement between Cd and S parallel to the surface plane, and d_{12}, the distance perpendicular to the surface between the top Cd and the second-layer S (all defined in Fig. 1) are considerably more complex on this surface than on the zinc-blende-structure (110) or wurtzite-structure (10$\bar{1}$0) surface, and cannot be presented in compact form. The calculation of the x, y, and z coordinates of each surface atom as a function of ω is presented in Appendix B. The bond-length-conserving relaxations induce a puckering of the surface unit cell, as indicated in Fig. 4. Unlike the zinc-blende-structure (110) and wurtzite-structure (110) and wurtzite-structure (10$\bar{1}$0) surfaces, for which the observed $I(hk)=I(\bar{h}k)$ symmetry indicates that surface atomic relaxations are confined to the (y,z) plane, for the wurtzite-structure (11$\bar{2}$0) surface the glide-plane symmetry permits arbitrary displacements of the one independent pair of Cd and S species in the unit cell. The resulting local structure of the surface anion-cation-anion triplets is analogous to that obtained on the (110) zinc-blende surface.

The initial stage of the structure search consisted of minimizing R_X and R_I with respect to ω. LEED intensities were calculated for a range of bond-length-conserving relaxations described by $0°<\omega<40°$ in steps of 5° for most of the range, and 2° near the R-factor minima. The results are summarized in panel (a) of Fig. 5. Two R_X minima are found: 0.27 for $\omega=0°$ and 0.25 for $\omega=30°$. Previous LEED structure determinations have shown that significantly different qualities of fit between experimental and calculated I-V profiles correspond to R_X values that differ by more than 0.02.[13] Thus, on the basis of R_X alone, the $\omega=0°$ and 32° structures provide similar fits and one cannot be favored over the other. R_I, however, with values of 0.28 for $\omega=0°$ and 0.095 for $\omega=32°$, provides a clear preference for the second structure. The corresponding I-V profiles of several representative beams are displayed in Fig. 6. The low value of R_I for $\omega=32°$ indicates that the calculation reproduces satisfactorily the relative strength of these beams. The bond-length-conserving top-layer rotation characterized by $\omega=32°$ is specified in Table I.

This structure was used as the starting point for further refinements. First, the first-to-second-layer spacing, characterized by $d_{12\perp}$, was changed by $-0.14<\delta d_{12\perp}<0.08$ Å. An R_X minimum equal to 0.21 and a value of R_I equal to 0.08 were found for $\delta d_{12\perp}=-0.1$ Å [Fig. 5(b)]. This bond rotation plus contraction produces a

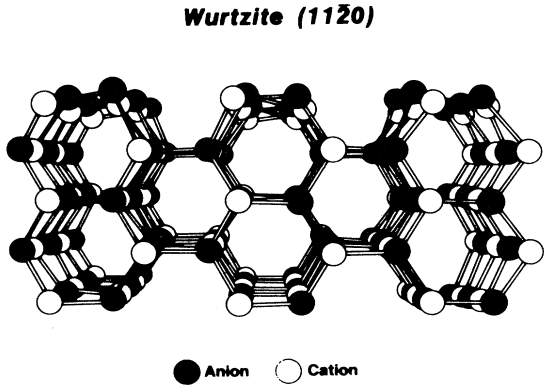

FIG. 4. Drawing of the relaxed (11$\bar{2}$0) CdS surface.

$\delta R_X = -0.03$ and corresponds therefore to a significant improvement in the description of the experiment by the theory over that obtained for the bond-length-conserving rotation. To insure internal consistency in the structure determination process, ω was reoptimized with the 0.1-Å first-to-second-layer contraction built in the structure. An R_X minimum equal to 0.21 was found for $\omega = 30°$ while R_I assumed the same value as before [Fig. 5(c)]. Note that the 0.1-Å contraction provides a clear discrimination in the R_X curve between the $\omega = 0°$ and 30° structures. The I-V profiles corresponding to this minimum R_X structure are displayed in Fig. 7. In this structure, the length of the surface Cd—S bonds is conserved but the bond length of the surface Cd (S) to second-layer S (Cd) bonds is contracted by about 2.3%. The parameters of this "best-fit" structure are specified in Table I. Finally, this structure was used as the starting point for optimizing Δ_{21}, the second-layer shear. Given the insensitivity of the calculation to atomic displacements parallel to the surface plane in the second and deeper layers, Δ_{21} was obtained by displacing Cd and S only in the direction perpendicular to the surface and symmetrically with respect

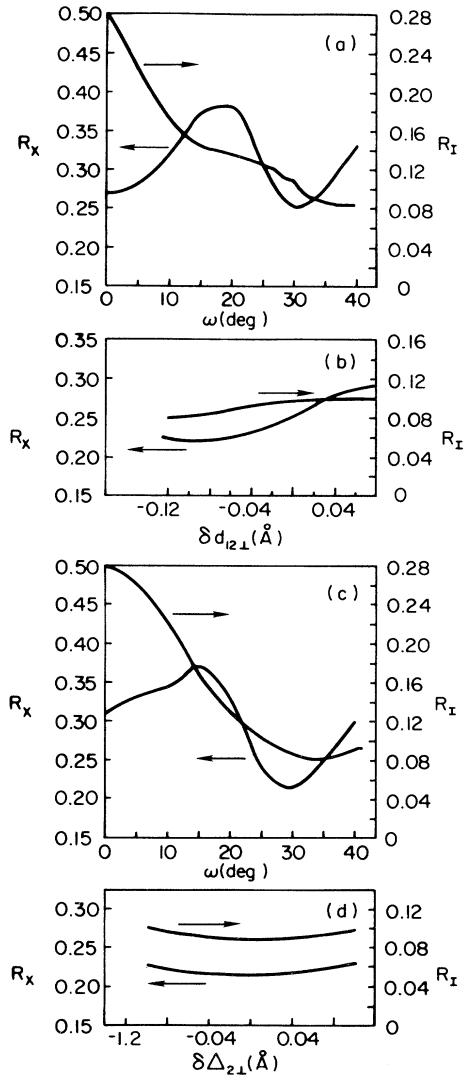

FIG. 5. Values of the R factors R_X and R_I associated with the systematic variations of the parameters defining the atomic structure of the $(11\bar{2}0)$ surface. The parameters are defined in Fig. 1. (a) ω scan for bond-length-conserving rotations in the top layer; (b) $\delta d_{12\perp}$ scan with $\omega = 32°$, the bond rotation corresponding to the R_X minimum in (a); (c) ω scan with $\delta d_{12\perp} = -0.1$ Å, the first-to-second- layer contraction optimized in (b); (d) Δ_{21} scan with the other parameters optimized in (a)–(c).

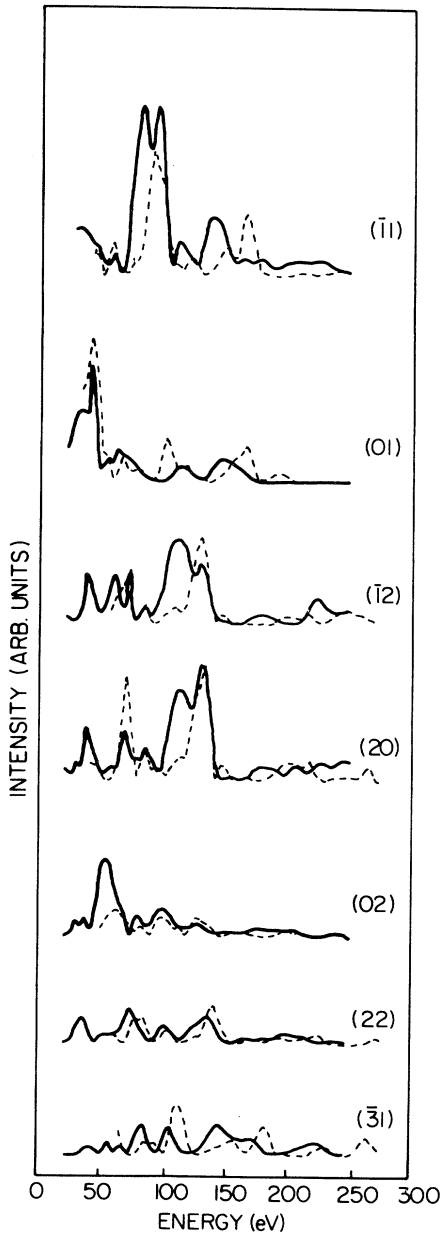

FIG. 6. Same as Fig. 3 with calculated I-V curves corresponding to the bond-length-conserving rotation $\omega = 32°$, which leads to the minimum R_X in Fig. 4(a).

to the second-layer plane. This distortion, however, did not produce any further improvement in the fit between the measured and calculated intensities [Fig. 5(d)].

Following the structure search, we investigated the impact of nonstructural parameters on the description of experimental *I-V* profiles by the theory. A substantially improved value of the minimum R_X equal to 0.175 was obtained by extending the calculation to a slab of seven layers (versus six) and four layers calculated exactly (versus three in the previous calculations). R_I was also improved (0.075), although less significantly. No significant improvement was obtained by varying the inelastic mean free path λ_{ee}. To insure consistency in the structure determination process, we also performed a limited search for ω, $d_{12\perp}$, and $\Delta_{2\perp}$ using these nonstructural parameters. The unrelaxed geometry led to values of R_X and R_I equal to 0.25 and 0.24, respectively, and no change was obtained in the best-fit structure. The *I-V* profiles corresponding to the best-fit structure and to the revised nonstructural parameters are compared with the measured intensities in Fig. 8.

The best R_X values obtained above, which are higher

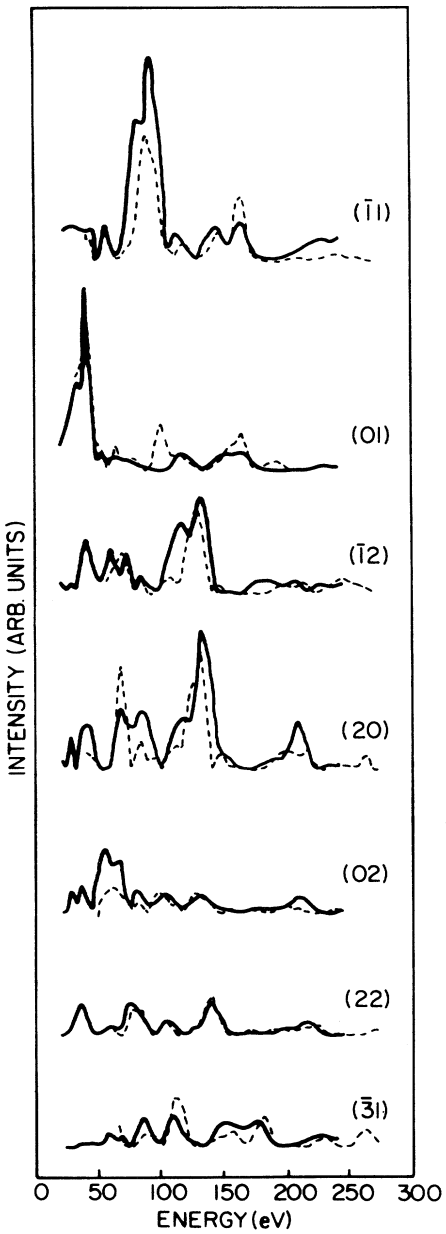

FIG. 7. Same as Fig. 3 with calculated *I-V* curves corresponding to the bond-length-conserving rotation $\omega=30°$ plus $\delta d_{12\perp}=-0.1$ Å contraction to the first-to-second layer spacing, which leads to the minimum R_X in Fig. 5(c).

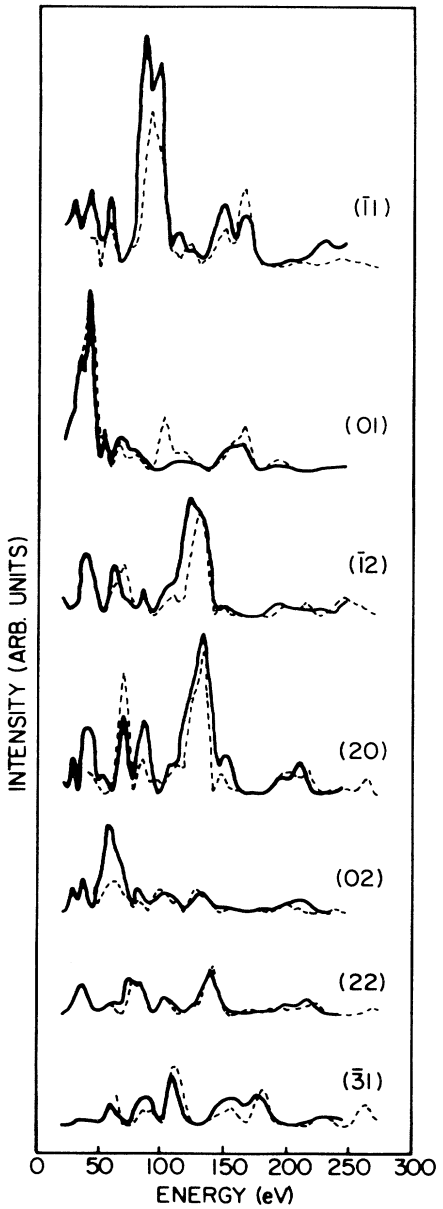

FIG. 8. Same as Fig. 7 with a calculation extended to six phase shifts, a seven-layer slab, and four layers calculated exactly.

than those generally obtained in LEED work on metal surfaces, should be placed in perspective. The quality of the fit between calculated and measured LEED intensities is limited in part by experimental and theoretical problems. The former are mainly due to varying degrees of reproducibility in the data-collection process. Variations in the quality of compound semiconductor surfaces prepared by cleaving or sputtering and annealing have been shown to produce R_X values of the order of 0.1 (Ref. 14) for comparison of independent sets of data. This constitutes a first lower bound for the best-fit R factor between calculated and measured intensities, independent of the structure determination. The theoretical limitations stem from the necessary approximations used in the description of the electron solid force law and scattering potential. The spherical-averaging and muffin-tin approximations of the scattering potential, for example, introduce larger discrepancies for binary compounds, in which bonding is directional, than for metals, in which the scattering potential is more spherical.

These limitations affect the quality of the fit between calculated and measured intensities in compound semiconductor work, and confine R_X to values above 0.1. Yet, they have been shown not to have a significant impact on the atomic geometry determined in the process.[12,15] The best R_X value presented above, i.e., 0.175, is equivalent to the best R_X obtained for the (110) surfaces of III-V and II-VI zinc-blende-structure compounds,[16] the structures of which have been confirmed with techniques other than LEED and are accepted as the standard in the field. It represents a state-of-the-art structure determination for a compound semiconductor surface.

V. SUMMARY AND DISCUSSION

The most significant result obtained in this analysis is the demonstration that the atomic geometry of the CdS(11$\bar{2}$0) surface is relaxed with respect to the geometry of the truncated-bulk crystal. The Cd-S shear perpendicular to the surface in the top layer ($\Delta_{1\perp}=0.65$ Å) is a large fraction of the (11$\bar{2}$0) interplanar distance (2.07 Å). The analysis produces values of R_X and R_I that are equivalent to the lowest obtained from previous LEED structure determinations on tetrahedrally coordinated III-V and II-VI compounds, including CdSe(11$\bar{2}$0). These low values, which are in part due to the high quality of the data taken with our fast LEED data-acquisition system, generate a high level of confidence in the structure analysis.

The atomic geometry of CdSe(10$\bar{1}$0) (Ref. 1) was recently compared with that of ZnO(10$\bar{1}$0) determined by LEED over a decade ago,[14] and the two were found to be compatible. A significant aspect of our present work is that it provides the first comparison between atomic geometries of the (11$\bar{2}$0) surfaces of two different wurtzite-structure compounds CdSe and CdS determined with a modern LEED computation technology that affords a considerably higher level of accuracy in the data taking, in the definition of the scattering potentials, and in the systematic structure search via R-factor analysis. In this respect, the CdS surface structure described above is found to be qualitatively similar to the CdSe(11$\bar{2}$0) structure determined by LEED as well as low-energy positron diffraction (LEPD).[2,5] These results suggest that the (11$\bar{2}$0) surfaces of wurtzite-structure compound semiconductors may also exhibit a universal surface structure when the independent structural variables scaled with the bulk lattice constant, as has already been well established for the cleavage (110) surface of zinc-blende-structure III-V and II-VI compounds[4] and was recently predicted to occur for the (10$\bar{1}$0) and (11$\bar{2}$0) surfaces of wurtzite-structure compounds.[3] Specifically, it was predicted that, on the (11$\bar{2}$0) surfaces of ZnO, ZnS, ZnSe, CdS, and CdSe, the first-layer vertical shear normalized to the lattice constant, $\Delta_{1\perp}/a_0$, remains approximately equal to 16.5%. Our LEED analysis yields 15.6%. Furthermore, the local atomic structure displayed at these (11$\bar{2}$0) surfaces is very similar to that found at (110) zinc-blende-structure surfaces: the surface bond rotation results in the anion moving away from the bulk and assuming a p^3-like configuration, and the cation moving toward the plane defined by its three anion neighbors and assuming an sp^2-like configuration. The similarity in the local structure of widely different materials such as covalent zinc-blende-structure III-V compounds such as InSb and more ionic wurtzite-structure II-VI compounds such as CdS demonstrates that small molecule coordination chemistry alone does not suffice to determine the atomic structure of these surfaces. Total-energy calculations have shown that the bond-rotation relaxations found on zinc-blende-structure (110) and wurtzite-structure (10$\bar{1}$0) and (11$\bar{2}$0) cleavage surfaces are driven by the lowering of the surface-state energy. These calculations reveal that the "dangling-bond" surface gap states associated with the truncated-bulk structure on cleavage wurtzite-structure surfaces are eliminated by the bond-length-conserving rotation, become surface resonances that exhibit back-bonding character. The concomitant lowering of the surface electronic energy is sufficient to balance the energy increase due to the elastic deformation of surface bonds. It becomes, therefore, the driving force behind this atomic relaxation and is confined to second-order-effect differences between the relaxations exhibited by different materials due to ionicity or to other details of the electronic potential.

The CdS structure determined in this paper is in good agreement with that predicted by total-energy minimization (bottom row in Table I). The predicted structure is a bond-length-conserving relaxation obtained by letting first- and second-layer atoms move freely while minimizing the total surface energy.[3] The main difference revealed by Table I is that the calculation predicts a second-layer relaxation ($\Delta_{2\perp}=0.1$ Å) whereas the LEED analysis does not. Yet, the R_X vs $\Delta_{2\perp}$ curve [Fig. 5(d)] is sufficiently flat that the existence of a small second-layer relaxation ($-0.05\leq\Delta_{2\perp}\leq0.05$ Å) cannot be ruled out by the LEED analysis. The degree of agreement is also comparable to that achieved for the well-understood (110) surfaces of III-V compounds.[4] The similarity between predicted and measured structures, obtained with independent techniques that explore the structural parame-

ter space in different ways, brings a high level of confidence in the modern LEED structure determination process.

ACKNOWLEDGMENT

This work was supported by National Science Foundation Grant No. DMR-87-09531.

APPENDIX A: SYMMETRY OF THE DIFFRACTION ON THE (11$\bar{2}$0) SURFACE

The diffraction pattern from a truncated bulk wurtzite-structure (11$\bar{2}$0) surface is characterized by an $I(hk)=I(h\bar{k})$ symmetry, and by the fact that the $(h0)$ beams are missing for h odd, as shown below. Both results are consequences of a glide-plane symmetry characteristic of the chains of atoms that lie in and parallel to the (11$\bar{2}$0) surface. We indicate below, using kinematic theory, that these relationships remain valid for surface relaxations that preserve the glide-plane symmetry characteristic of the bulk wurtzite-structure lattice. In a complete dynamical theory, the glide-plane symmetry is reflected in the identity of the scattering amplitudes of geometrically equivalent subplanes of scatterers parallel to the (11$\bar{2}$0) surface. The equality of these scattering amplitudes has been verified numerically for surface relaxation models that exhibit the glide-plane symmetry as described in Eq. (A1)–(A3) below. Therefore the analysis given below is valid for the dynamical theory as well when the scattering potentials V_A and V_B in Eqs. (A4) and (A5) are replaced by self-consistent subplane scattering amplitudes, which are obtained by the solution of the multiple-scattering equations. These amplitudes are different within each individual layer of the lattice parallel to the (11$\bar{2}$0) surface, but they exhibit the symmetry of V_A and V_B in Eqs. (A4) and (A5), and hence the demonstration given below for the top layer alone is valid layer by layer in the complete dynamical theory.

Whether the observed surface relaxation exhibits the glide-plane symmetry characteristic of the bulk lattice is a matter for experimental determination. Since the resulting missing beams and $I(hk)=I(h\bar{k})$ symmetry are observed, however, we infer that glide-plane symmetry does characterize the surface relaxations. Hence, we utilize the associated geometrical restrictions to reduce the number of independent structural variables in our determination of the surface atomic geometry of CdS(11$\bar{2}$0).

Consider the schematic of the undistorted unit cell shown in panel (a) of Fig. 9. Atoms (1) and (3) are of type A, atoms (2) and (4) of type B. Next to each atom is a set of x and y coordinates that indicates its position with respect to the origin midway between atoms (2) and (3). The glide-plane symmetry consists of the invariance of the structure by a translation by $a_x/2$ along the x axis followed by a reflection through a plane normal to the y axis passing through the origin. This symmetry implies the following relationships between the displacements $(\Delta x_i, \Delta y_i, \Delta z_i)$ of the ith surface atom from its position in the truncated-bulk structure:

$$\Delta x_1=\Delta x_3=\alpha_1 a_x \ , \tag{A1a}$$

$$\Delta x_2=\Delta x_4=\alpha_2 a_x \ , \tag{A1b}$$

$$\Delta y_1=-\Delta y_3=\beta_1 a_y \ , \tag{A2a}$$

$$\Delta y_2=-\Delta y_4=\beta_2 a_y \ , \tag{A2b}$$

$$\Delta z_1=\Delta z_3=\Delta z_A \ , \tag{A3a}$$

$$\Delta z_2=\Delta z_4=\Delta z_B \ . \tag{A3b}$$

Using Eqs. (A1)–(A3) and Fig. 9 to calculate the structure factor for the top layer of the relaxed wurtzite-structure (11$\bar{2}$0) surface we obtain

$$\begin{aligned} S(h,k)=&V_A \exp(2ik_\perp \Delta z_A)\{\exp[(-\tfrac{7}{8}+2\alpha_1)\pi ih]\exp[(-\tfrac{1}{3}+2\beta_1)\pi ik]+\exp[(\tfrac{1}{8}+2\alpha_1)\pi ih]\exp[(\tfrac{1}{3}-2\beta_1)\pi ik]\} \\ &+V_B \exp(2ik_\perp \Delta z_B)\{\exp[(-\tfrac{1}{8}+2\alpha_2)\pi ih]\exp[(-\tfrac{1}{3}+2\beta_2)\pi ik]+\exp[(\tfrac{7}{8}+2\alpha_2)\pi ih]\exp[(\tfrac{1}{3}-2\beta_2)\pi ik]\} \end{aligned} \tag{A4}$$

in which V_A and V_B are the scattering potentials of the A and B species, $k_\perp$ is the momentum normal to the surface, and (hk) designate the indices of the diffracted beams as indicated in Fig. 1. Since h is an integer, we can rewrite Eq. (A4) as

$$\begin{aligned} S(hk)=&V_A \exp(2ik_\perp \Delta z_A)\exp[(\tfrac{1}{8}+2\alpha_1)\pi ih]\{\exp[(\tfrac{1}{3}-2\beta_1)\pi ik]+(-1)^h\exp[-(\tfrac{1}{3}-2\beta_1)\pi ik]\} \\ &+V_B \exp(2ik_\perp \Delta z_B)\exp[(\tfrac{7}{8}+2\alpha_2)\pi ih]\{\exp[(\tfrac{1}{3}-2\beta_2)\pi ik]+(-1)^h\exp[-(\tfrac{1}{3}-2\beta_2)\pi ik]\} \ . \end{aligned} \tag{A5}$$

Equation (A5) shows that if $k=0$, then $S(h,0)$ is proportional to the factor $[1+(-1)^h]$ indicating that

$$S(h,0)=0, \quad h=\text{odd} \ . \tag{A6a}$$

Moreover, Eq. (A5) reveals that

$$S(h,-k)=S(h,k), \quad h=\text{even} \ ,$$

$$S(h,-k)=-S(h,k), \quad h=\text{odd} \ ,$$

so that

$$I(h,k)=|S(h,k)|^2=I(h,-k) \tag{A6b}$$

for all values of h and k. Equations (A6) constitute the desired results of the consequences of the preservation of glide-plane symmetry in the top layer. As noted above, in a dynamical multiple scattering, V_A and V_B are replaced by the self-consistent subplane scattering amplitudes and the analysis remains valid layer by layer.

APPENDIX B: ANALYSIS OF (11$\bar{2}$0) BOND-LENGTH-CONSERVING TOP-LAYER RELAXATIONS

As discussed previously for the (110) surfaces of zinc-blende-structure materials[4] and the (10$\bar{1}$0) surfaces of CdSe,[1,2] a remarkable feature of the cleavage surfaces of tetrahedrally coordinated compound semiconductors is the fact that large relaxations of their atomic geometries can occur without the distortion of any bond lengths from their bulk values. For zinc-blende-structure (110) and wurtzite-structure (10$\bar{1}$0) surfaces, these relaxations may be characterized as rigid rotations of the plane of the surface layer described by a single angular parameter ω giving the tilt between the relaxed and truncated-bulk surfaces planes.[1,2,4] For the wurtzite-structure (11$\bar{2}$0) surface the relaxations are more complicated, however, involving a puckering of the surface layer with the anion relaxing outward and the anion inward. Two angular variables characterize these relaxations, e.g., the angle ω_C between local anion-cation-anion planes and the surface normal and that between local cation-anion-cation planes and the surface normal, ω_A. In this appendix, we derive expressions for the structural parameters associated with these rotations for use in our LEED structural searches. Specifically, we use $\omega=\omega_C$ as the independent structural variable and constrain ω_A so that a convenient constitutive equation is satisfied.

The nature of the bond-length-conserving relaxation is determined by the constraints satisfied by the surface species. The observed glide-plane symmetry of the surface renders the cations and anions in the surface symmetry equivalent, as shown in Appendix A. Thus, as indicated in Fig. 9, we take atom (1) as the independent anion (S) and atom (2) as the independent cation (Cd) so $z_1 > z_2$. The origin may be selected at the second-layer cation (Cd) bonded to atom (1), as shown in panel (b) of Fig. 9. The parameters defined in Fig. 9 may then be evaluated with reference to the bulk wurtzite-structure lattice.

The positions of the surface atoms are characterized by six independent structural variables (x_1,y_1,z_1) and (x_2,y_2,z_2), but only four independent constraints. The first of these is the constraint on the bond length between atoms (1) and (2) in the surface, e.g.,

$$(x_1-x_2)^2+(y_1-y_2)^2+(z_1-z_2)^2=d^2 \tag{B1a}$$

in which d is the Cd—S bond length. The second is that between atom (1) and atom (4) in the unit cell beneath. Using the glide-plane equivalences discussed in Appendix A, we find

$$(x_1-x_2+a_x/2)^2+(2\gamma-y_1-y_2)^2+(z_1-z_2)^2=d^2 \tag{B1b}$$

in which a_x is the bulk unit-cell dimension along the hexagonal axis and γ is the displacement between the origins in panels (a) and (b) of Fig. 9. In terms of panel (b) of Fig. 9, $\gamma=a_y/6+t/2$ where $t^2=(a_x d-a_x^2/4)$ and a_y is the bulk unit-cell dimension perpendicular to the hexagonal axis. The third is the constraint on the back bond from atom (1), i.e.,

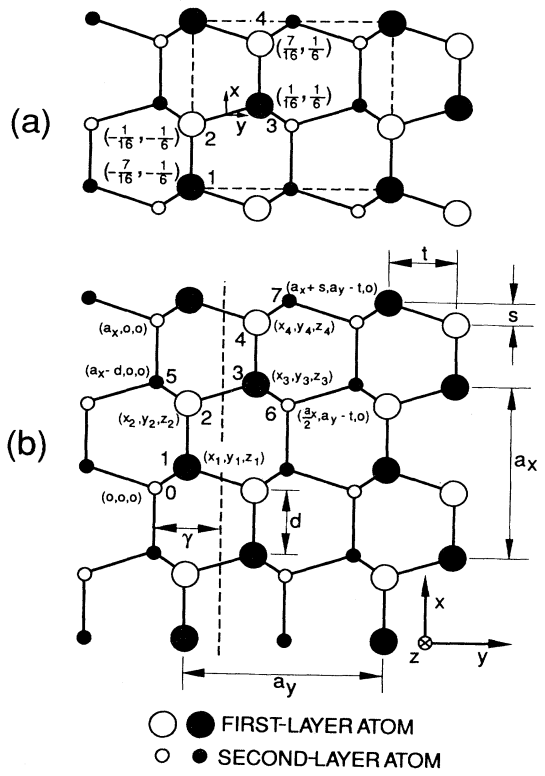

FIG. 9. Top view of the (11$\bar{2}$0) surface. (a) The coordinates of each surface atom are given in units of unit-cell dimensions, relative to the origin placed midway between (2) and (3) (Appendix A); the unit cell is drawn in dotted lines; (b) the position and (x,y,z) coordinates of each surface and second-layer atom entering the calculation of the relaxation as a function of ω (Appendix B).

$$x_1^2+y_1^2+z_1^2=d^2\ , \tag{B1c}$$

and the fourth is that on the back bond from atom (2):

$$(x_2-a_x+d)^2+y_2^2+z_2^2=d^2\ . \tag{B1d}$$

These four equations plus two constitutive equations defining two independent angular variables, e.g., ω_C and ω_A, define the structural parameters (x_1,y_1,z_1) and (x_2,y_2,z_2) associated with bond-length-conserving top-layer relaxations for the wurtzite-structure (11$\bar{2}$0) surface.

As noted earlier, for the purpose of achieving a single-parameter initial bond-length-conserving structural search, we select $\omega=\omega_C$ as the independent structural variable and replace the definition of ω_A with a constitutive relation that renders ω_A a function of $\omega=\omega_C$. Specifically, we use the definition of ω to write x_2 as a functional of ω and constrain x_1 to be a function of ω via $x_1=s-0.45\tan\omega$ in which $s=(a_x/2-d)$. Equations (B1a)–(B1d) are then solved by an iterative process to obtain the remaining four independent variables (y_1,z_1,y_2,z_2). Specifically, this procedure leads to four equations:

$$y_2=\gamma-\frac{\cos\omega}{2^{1/2}}\{B-[B^2-(a_x^2/4)(1+\tan^2\omega)\times(x_2-x_1-a_x/4)^2]^{1/2}\}^{1/2}\ , \tag{B2a}$$

$$B=\frac{a_x}{2}(x_2-x_1-a_x/4)+d^2-(x_2-x_1)^2-(\tan^2\omega)(x_2-x_1-a_x/4)^2\ , \tag{B2b}$$

$$y_1=\gamma-\frac{a_x}{4(\gamma-y_2)}(x_2-x_1-a_x/4)\ , \tag{B3}$$

$$z_2=[d^2-(x_2-a_x+d)^2-y_2^2]^{1/2}\ , \tag{B4}$$

$$z_1=z_2+[(\gamma-y_2)^2+(x_2-x_1-a_x/4)^2]^{1/2}\tan\omega\ , \tag{B5}$$

from the definitions of ω and Eqs. (B1a), (B2b), and (B1d). These are solved iteratively by taking $x_2=a_x/2$ initially and iterating in steps of 2×10^{-6} Å until Eq. (B1c) is satisfied to with $\pm10^{-2}$ Å. The resulting values of (x_1,y_1,z_1) and (x_2,y_2,z_2), plus utilization of the glide-plane symmetries described in Appendix A to obtain (x_3,y_3,z_3) and (x_4,y_4,z_4), are used to construct files for the LEED intensity calculations, the results of which are described in the text.

[1]C. B. Duke, A Paton, Y. R. Wang, K. Stiles, and A. Kahn, Surf. Sci. **197**, 11 (1988).
[2]T. N. Horsky, G. R. Brandes, K. F. Canter, C. B. Duke, S. F. Horng, A. Kahn, D. L. Lessor, A. P. Mills, Jr., A. Paton, K. Stevens, and K. Stiles, Phys. Rev. Lett. **62**, 1876 (1989).
[3]Y. R. Wang and C. B. Duke, Phys. Rev. B **37**, 6417 (1988).
[4]C. B. Duke, in *Surface Properties of Electronic Materials,* edited by D. A. King and D. P. Woodruff (Elsevier, Amsterdam, 1988), pp. 69–118.
[5]C. B. Duke, D. L. Lessor, T. N. Horsky, G. Brandes, K. F. Canter, P. H. Lippel, A. P. Mills, Jr., A. Paton, and Y. R. Wang, J. Vac. Sci. Technol. A **7**, 2030 (1989).
[6]R. J. Meyer, C. B. Duke, A. Paton, A. Kahn, E. So, J. L. Yeh, and P. Mark, Phys. Rev. B **19**, 5194 (1979).
[7]G. E. Laramore and C. B. Duke, Phys. Rev. B **5**, 267 (1972).
[8]S. Hara, J. Phys. Soc. Jpn. **22**, 710 (1967).
[9]W. K. Ford, C. B. Duke, and A. Paton, Surf. Sci. **115**, 195 (1982).
[10]C. B. Duke, Adv. Chem. Phys. **27**, 1 (1974).
[11]E. Zanazzi and F. Jona, Surf. Sci. **62**, 61 (1977).
[12]C. B. Duke, S. L. Richardson, and A. Paton, Surf. Sci. **127**, L135 (1983).
[13]C. B. Duke, W. K. Ford, A. Paton, A. Kahn, and J. Carelli, Phys. Rev. B **24**, 562 (1981).
[14]C. B. Duke, R. J. Meyer, A. Paton, and P. Mark, Phys. Rev. B **18**, 4255 (1978).
[15]C. B. Duke and A. Paton, Surf. Sci. **164**, L797 (1985).
[16]A. Kahn, Surf. Sci. Rep. **3**, 193 (1983).
[17]R. W. G. Wyckoff, *Crystal Structures* (Wiley, New York, 1963), Vol. 1, p. 112.